Kinetics of CH_3OH Oxidation on PtRu/C Studied by Impedance and CO Stripping Voltammetry

Wataru Sugimoto,* Kei Aoyama, Tomoyuki Kawaguchi, Yasushi Murakami, and Yoshio Takasu

Department of Fine Materials Engineering, Faculty of Textile Science and Technology, Shinshu University, 3-15-1 Tokida, Ueda 386-8567, JAPAN

* Corresponding author. Tel.: +81-268-21-5455; Fax: +81-268-22-9048
E-mail address: wsugi@shinshu-u.ac.jp (W. Sugimoto).

ABSTRACT

The kinetics of the CH_3OH oxidation reaction at 60°C on well-alloyed platinum-ruthenium supported on carbon ($Pt_{50}Ru_{50}$/C) was studied by electrochemical impedance spectroscopy and compared with carbon-supported platinum (Pt/C). The reaction rate of the overall CH_3OH oxidation increased with increasing electrode potential for both Pt/C and PtRu/C. In the case of Pt/C, when the electrode potential was $E \leq 450$ mV vs. RHE only a capacitive behavior was observed. Resistive and pseudo-inductive behaviors were evident above 500 and 600 mV vs. RHE. In the case of PtRu/C, a similar change in behavior was observed, except that the behaviors were observed at 200 mV lower electrode potentials than Pt/C. Correlation of the impedance data with pre-adsorbed carbon monoxide (CO_{ad}) stripping voltammetry allowed the understanding of the methanol oxidation reaction. The change in the reaction rate of the oxidation of CH_3OH to CO_{ad} as a function of the electrode potential as well as the promotion effect of Ru was evidenced by a change in the frequency where

the frequency deviates from the ~90° phase angle. The change in the reaction rate of the oxidation of CO_{ad} to CO_2 as a function of the electrode potential as well as the alloying with Ru was evidenced by a change in the frequency where the phase angle approached zero.

Keywords: Direct methanol fuel cell; CO stripping voltammetry; Electrochemical impedance spectroscopy; PtRu/C; electrocatalyst

1. Introduction

Binary PtRu/C is a promising anode catalyst for use in the direct-methanol fuel cell (DMFC) [1-18]. A series of reactions takes place on the Pt surface for CH_3OH oxidation, which can be simplified as below:

$$CH_3OH + Pt \rightarrow CO_{ad}\text{-}Pt + 4H^+ + 4e^- \quad [1]$$

$$CO_{ad}\text{-}Pt + Pt + H_2O \rightarrow CO_{ad}\text{-}Pt + OH_{ad}\text{-}Pt + H^+ + e^- \rightarrow 2Pt + CO_2 + 2H^+ + 2e^- \quad [2]$$

The CO_{ad} oxidation process (Eq. (2)) is postulated to be the rate-determining step. In the case of PtRu, CH_3OH oxidation can be summarized as below:

$$CH_3OH + PtRu \rightarrow CO_{ad}\text{-}PtRu + 4H^+ + 4e^- \quad [3]$$

$$CO_{ad}\text{-}PtRu + H_2O \rightarrow CO_{ad}\text{-}PtRu\text{-}OH_{ad} + H^+ + e^- \rightarrow PtRu + CO_2 + 2H^+ + 2e^- \quad [4]$$

Ru is widely known as a second metal that promotes the CH_3OH electro-oxidation [19]. The promotion effect has been mainly discussed based on the so-called "bifunctional effect" [16,20-48] or "ligand effect" [3,31-34,37,46-66] or a mixture of both [31-34,37,46,67,68]. The bifunctional mechanism, proposed by Watanabe and Motoo [20,21], proposes that Ru acts as a promoter for the oxidation of the strongly bound CO_{ad} on Pt by supplying an oxygen source ($Ru\text{-}OH_{ad}$). According to the ligand effect, the energy level of the catalyst is changed so that the binding strength of CO_{ad} is weakened, thus reducing the oxidation overpotential of the overall CH_3OH electro-oxidation.

In order to prepare active electrocatalysts, it is important that the fundamental electrocatalytic activity of CH_3OH and CO_{ad} oxidation is understood. In particular, for understanding reactions with different reaction rates, it is important that the kinetics

of the oxidation of CH_3OH is characterized. Electrochemical impedance spectroscopy is a powerful method to probe the kinetics of electrochemical reactions and has recently been utilized to understand the anodic processes for CH_3OH oxidation [68-75]. Using a membrane electrode assembly (MEA) with H_2 passed on the cathode side (instead of O_2 in DMFC) to act as the counter and reference electrode, Müller and co-workers examined the reaction kinetics and mass-transport taking place on the DMFC anode [69,70]. They proposed an equivalent circuit that explains the inductive behavior of the DMFC anode. Using a Pt thin-film electrode in a half-cell configuration, a faradaic impedance model for the CH_3OH oxidation was developed allowing a quantitative assessment of the change in the impedance behavior as a function of the electrode potential [73].

In this work, we studied the CH_3OH oxidation on Pt/C and well-alloyed PtRu/C by electrochemical impedance spectroscopy. The thin film electrode method [76,77] in a half-cell configuration was employed in this study the intrinsic behavior of the anodic process. Compared to studies with an MEA with H_2 passed on the cathode side, the effect of electrolyte resistance in the impedance data can be avoided and the anodic process can be probed quantitatively. The impedance data were correlated with voltammetry studies of the oxidation pre-adsorbed CO_{ad}. From the above data, the reaction kinetics taking place on Pt and PtRu are evaluated, and the promotion effect of Ru on CH_3OH oxidation is discussed.

2. Experimental

Pt/C (30 mass% Pt) and $Pt_{50}Ru_{50}$/C (30 mass% PtRu) electrocatalysts were prepared by an impregnation method reported previously [10-15]. Briefly, Pt/C and $Pt_{50}Ru_{50}$/C electrocatalysts were prepared by introducing appropriate amounts of Vulcan XC-72R into $Pt(NH_3)_2(NO_2)_2$ (Ishifuku Metal Industry Co.) dissolved in ethanol or a 1 : 1 molar ratio of $Pt(NH_3)_2(NO_2)_2$ and $Ru(NO_3)_3$ (Tanaka Kikinzoku Kogyo K.K.) dissolved in ethanol. After thorough mixing, the precursor solution was allowed to dry at 60°C. The product powder was then reduced in a tube furnace under flowing H_2(10%)-N_2(90%) gas for 2 h at 450°C. These conditions produce highly dispersed, well-alloyed particles with average particle size of c.a. 3 nm [10]. The overall surface area of the electrocatalysts was determined using the Brunauer-Emmett-Teller (BET) equation from N_2 adsorption/desorption measurements conducted with a Micromeritics ASAP2010 instrument.

The working electrode was prepared by the thin film electrode method [76,77], which is composed of a mirror polished Glassy Carbon rod (0.196 cm^2 surface) modified with 40 μg of the active material (12 μg metal) and 20 μL of a 1 wt% Nafion® solution to affix the electrocatalysts to the Glassy Carbon rod. A beaker-type electrochemical cell equipped with the working electrode, a platinum mesh counter electrode, and an Ag/AgCl reference electrode was used. A Luggin capillary faced the working electrode at a distance of 2 mm. All electrode potentials throughout the paper will be referred to the RHE scale. All electrochemical measurements were conducted at 60°C, corrected for the temperature effect.

Oxidation of pre-adsorbed carbon monoxide (CO_{ad}) was measured by CO_{ad}

stripping voltammetry in 0.5 M H_2SO_4 solution at a scan rate of 10 mV s^{-1}. Gaseous CO was purged into the cell (0.5 M H_2SO_4, 60°C) for 40 minutes to allow complete adsorption of CO onto the electrocatalysts while maintaining a constant voltage of 300 mV vs. RHE. Excess CO dissolved in the electrolyte was purged out with N_2 for at least 40 minutes. After the CO stripping voltammetry, 1 M CH_3OH was introduced into the cell and chronoamperometry was conducted at the desired electrode potential for 30 min to obtain a quasi-steady state. Impedance measurement was conducted immediately after chronoamperometry by sweeping frequencies from 5 000 to 0.050 Hz in a constant voltage mode at an amplitude of 10 mV at the desired electrode potential. The electrode potential was varied from 700 to 400 mV vs. RHE for Pt/C and 550 to 300 mV for PtRu/C.

3. Results and Discussion

The voltammograms of CO_{ad} oxidation on Pt/C and PtRu/C are shown in Fig. 1. The onset of CO_{ad} oxidation is observed at ~600 mV vs. RHE on Pt/C and at ~350 mV vs. RHE, indicating the promotion effect of the CO_{ad} oxidation by the alloying of Ru. (Eqs. 2 and 4).

---------- Figure 1 ----------

The complex-plane impedance plots of Pt/C in 0.5 M H_2SO_4 + 1 M CH_3OH at various electrode potentials from 200 mV negative to the CO_{ad} oxidation onset potential to 100 mV positive to the CO_{ad} oxidation onset potential (400, 450, 500, 550, 600, 650, and 700 mV vs. RHE) are shown in Fig. 2. At E = 400 and 450 mV vs. RHE, the

impedance shows a line with a slope close to 90° along the imaginary axis (Z''), characteristic of an ideally polarizable electrode as in an electrical double-layer capacitor. A slight deviation from the straight line is observed at low frequency (< 0.5 Hz), which may be an indication of the commencement of the dissociative methanol adsorption. At E = 500 and 550 mV vs. RHE, an arc is evident in the complex-plane plots, which indicates the presence of a resistive component. With a further increase in electrode potential ($E \geq$ 600 mV vs. RHE), a pseudo-inductive behavior is observed (positive Z'' values). This pseudo-inductive behavior has been attributed to CO_{ad} oxidation (Eq. 2) [70,73,74].

---------- Figure 2 ----------

The complex-plane impedance plots of PtRu/C in 0.5 M H_2SO_4 + 1 M CH_3OH at various electrode potentials from 50 mV negative to the CO_{ad} oxidation onset potential to 200 mV positive to the CO_{ad} oxidation onset potential (300, 350, 400, 450, 500, and 550 mV vs. RHE) are shown in Fig. 3. At E = 300 mV vs. RHE, an arc is already evident in the complex-plane plots. The pseudo-inductive behavior is clearly observed at $E \geq$ 400 mV vs. RHE. The frequency response of CH_3OH oxidation on PtRu/C is comparable to that on Pt/C at 200 mV lower electrode potentials, which indicates that the reaction rate of the overall oxidation of CH_3OH on PtRu/C and Pt/C is similar with a profit of 200 mV.

---------- Figure 3 ----------

The transition from the capacitive behavior to the resistive behavior and then to the pseudo-inductive behavior is more clearly evident in the corresponding Bode plots

(Figs. 4 and 5). The change from the capacitive to the resistive behavior can be distinguished by the characteristic frequency where the $-\phi$ value exhibits a maximum (designated as F_1), that is, the deviation from the –90° phase angle. The phase angle is almost constant down to 50 mHz when $E \leq 450$ mV vs. RHE for Pt/C. Therefore, the electrode reaction is dominated by the electrical double-layer capacitance and the electrocatalysis is small within the frequency range studied. A maximum in the $-\phi$ value in the Bode plots for Pt/C becomes apparent below ~0.80 Hz when $E = 500$ mV vs. RHE, and the characteristic frequency F_1 increases to higher frequency with increasing electrode potential. This implies increased reaction rates for the resistive behavior with increasing electrode potential.

---------- Figure 4 ----------

---------- Figure 5 ----------

The change in the kinetics of the pseudo-inductive behavior can be distinguished from the characteristic frequency where the phase angle nears zero (designated as F_2). Zero phase angles are observed above 600 mV vs. RHE for Pt/C and above 400 mV vs. RHE for PtRu/C. With increasing electrode potential, the characteristic frequency F_2 increases to higher frequency. The increasing F_2 values as a function of the electrode potential suggests an increase in the reaction rate of the pseudo-inductive behavior with increasing electrode potential.

The transition frequencies, F_1 and F_2, for Pt/C and PtRu/C are plotted in Fig. 6 as a function of the applied electrode potentials. The F_1 and F_2 values are both higher for PtRu/C compared to Pt/C at the same the electrode potentials. Figure 6 also

implies that the reaction kinetics for Pt/C is comparable to PtRu/C at 200 mV lower potential.

---------- Figure 6 ----------

The voltammograms of CO_{ad} oxidation on Pt/C and PtRu/C (Fig. 1) corresponds well with the electrode potential where the pseudo-inductive behavior was observed; namely, above 600 mV vs. RHE for Pt/C and above 400 mV vs. RHE for PtRu/C. The electrode reactions taking place below the CO_{ad} oxidation threshold (below 600 mV vs. RHE for Pt/C and 400 mV vs. RHE for PtRu/C) should involve the oxidation of CH_3OH without the participation of surface hydroxyls. Therefore, the resistive behavior observed in the impedance data can be recognized as the reaction resistance of CH_3OH to CO_{ad} (Eqs. 1 and 3).

The methanol oxidation reaction should involve many parallel processes with reaction intermediates. In this study, the impedance data was analyzed assuming two major reactions; namely the CH_3OH to CO_{ad} and CO_{ad} to CO_2 oxidation reactions. The impedance data was initially fitted using an equivalent circuit shown in Fig. 7a, where R_s, C, R_∞, R_0, and L are the solution resistance, C is the capacitance, R_∞ is the reaction resistance of CH_3OH to CO_{ad}, R_0 is the reaction resistance of CO_{ad} oxidation, and L is the inductance of CO_{ad} oxidation [70,73,74]. Although the inductive behavior could be expressed using this model circuit, a distortion of the spectrum was observed. Such a distortion has been observed previously, and was attributed to the roughness of the catalytic layer or a current constriction effect [70,73,74]. A close examination of the high frequency data revealed that the impedance data was

independent of the electrode potential between 5 kHz to 50 mHz, suggesting that this frequency range is due to a charge transfer process at the outer most surface of the electrode. Thus, a parallel constant-phase element (CPE_1)-resistor (R_{ct}) combination was added in series to fit the high frequency impedance data (Fig. 7b) assuming a reaction step with a different time constant. Here, CPE_1 and R_{ct} are the frequency dependent capacitance and charge-transfer resistance at the outer most surface of the electrode. A constant phase element (CPE_2) was also used instead of a capacitor for the electrical double-layer capacitance to account for the porous PtRu/C. The fit (solid lines in Figs. 1-4) based on the modified equivalent circuit (Fig. 7b) agrees well with the experimental data throughout the whole frequency range studied. The value of CPE_2 was in the range of 7-9 μF cm^{-2} (per S_{BET} of Pt/C and PtRu/C; 214 m^2 $(g\text{-}Pt/C)^{-1}$ and 201 m^2 $(g\text{-}PtRu/C)^{-1}$), which is a reasonable value for the electrical double-layer capacitance. The reaction resistance R_0 and the inductance L of CO_{ad} oxidation decreased with increasing electrode potential, which can be attributed to the faster reaction rate of CO_{ad} oxidation to CO_2 (Eqs. 2 and 4) at higher electrode potentials. The plot of the R_0 and L values as a function of the electrode potential clearly shows that PtRu/C has an advantage in CO_{ad} oxidation of 150 to 200 mV (Fig. 8) compared to Pt/C, which is in agreement with the CO_{ad} stripping voltammetry results. The reaction resistance of CH_3OH to CO_{ad} (R_∞) also decreases with the increase in electrode potential. An important point to note is that R_∞ is not the same for Pt/C and PtRu/C: PtRu/C has an advantage of 150 to 200 mV over Pt/C.

---------- Figure 7 ----------

---------- Figure 8 ----------

The impedance data for the CH_3OH oxidation (Fig. 3) and CO_{ad} stripping voltammetry on PtRu/C (Fig. 1) reveals a reaction resistance at electrode potentials lower than the onset of CO_{ad} oxidation. The resistive behavior may be due to the reaction resistance of the dehydrogenation reaction and/or the oxidation process of intermediates. Since such reactions proceeds without the participation of surface hydroxyls ($Ru\text{-}OH_{ad}$), the bi-functional effect is an unlikely explanation for the promotion effect of Ru. A large contribution from the ligand effect (change in the electronic state) or a geometric effect (change in metal-metal distances) is a more likely cause for the change in the kinetics of such reactions.

Based on in-situ FTIR spectroscopy with the attenuated total reflection technique, Yajima et al. has shown that the CH_3OH dehydrogenation reaction takes place at an electrode potential as low as 100 mV vs. RHE at room temperature [22]. Since $Ru\text{-}OH_{ad}$ is not involved in the dehydrogenation of CH_3OH (Eq. 4), the increased reaction kinetics in the dehydrogenation of CH_3OH on PtRu/C compared to Pt/C (Eq. 1) is likely due to a ligand effect (change in electronic state) or a geometric effect (change in metal-metal distances). The profit of 200 mV in the oxidation of reaction intermediates seems quite large if there is no participation of $Ru\text{-}OH_{ad}$ (bi-functional mechanism). Lu and Masel have shown that the ligand effect contributes to only 1/3 to 1/5 of the CO removal in PEFC [78]. Liu and Nørskov suggests that the weaker bonding of CO with Pt on a PtRu surface is the main cause of the Ru promotion effect in PEFC, that is, the ligand effect is the major contribution [79]. Obviously, the

differences in the experimental protocols must be considered, and factors such as the temperature effect, methanol concentration, catalysts loading, etc. must be considered before a conclusive statement is made on the contribution of the ligand effect for the $CH_3OH \rightarrow CO_{ad}$ oxidation reaction. Such issues necessary to understand the CH_3OH oxidation reaction at low potentials are currently under investigation.

4. Conclusions

The kinetics of the CH_3OH on Pt/C and well-alloyed PtRu/C was studied by electrochemical impedance spectroscopy and CO_{ad} stripping voltammetry. The reaction rate of the overall CH_3OH oxidation was enhanced by alloying Pt and Ru, and CH_3OH oxidation on PtRu/C was approximately 200 mV lower compared to Pt/C. A model equivalent circuit was proposed to explain the impedance data, which enabled the extraction of the reaction kinetics of the oxidations of CH_3OH to CO_{ad} and CO_{ad} to CO_2. It was found that alloying of Pt and Ru enhanced the reaction rates of both CH_3OH to CO_{ad} and CO_{ad} to CO_2. The enhancement in the reaction rate of the CH_3OH oxidation by the alloying with Ru is likely due to a change in the electronic state of Pt with the alloying of Ru or a change in the metal bonding distance.

Acknowledgements

This work was supported in part by a Polymer Electrolyte Fuel Cell Program from the New Energy and Industrial Technology Development Organization (NEDO) of Japan, in collaboration with Toray Industries, Inc.

References

[1] B.D. McNicol, R.T. Short, J. Electroanal. Chem. 81 (1977) 249.

[2] M. Watanabe, M. Uchida, S. Motoo, J. Electroanal. Chem. 229 (1987) 395.

[3] J.B. Goodenough, A. Hamnett, B.J. Kennedy, R. Manohara, S.A. Weeks, J. Electroanal. Chem. 240 (1988) 133.

[4] A. Hamnett, S.A. Weeks, B.J. Kennedy, G. Troughton, P.A. Christensen, Ber. Bunsen-Ges. Phys. Chem. 94 (1990) 1014.

[5] A.S. Aricò, P. Creti, H. Kim, R. Mantegna, H. Giordano, V. Antonucci, J. Electrochem. Soc. 143 (1996) 3950.

[6] C. He, H.R. Kunz, J.M. Fenton, J. Electrochem. Soc. 144 (1997) 970.

[7] A.S. Aricò, A.K. Shukla, K.M. El-Khatib, P. Creti, V. Antonucci, J. Appl. Electrochem. 29 (1999) 671.

[8] T.J. Schmidt, H.A. Gasteiger, R.J. Behm, Electrochem. Commun. 1 (1999) 1.

[9] A.S. Aricò, P. Creti, E. Modica, G. Monforte, V. Baglio, Antonucci, V. Electrochim. Acta 45 (2000) 4319.

[10] Y. Takasu, T. Fujiwara, Y. Murakami, K. Sasaki, M. Oguri, T. Asaki, W. Sugimoto, J. Electrochem. Soc. 147 (2000) 4421.

[11] Y. Takasu, H. Itaya, T. Iwazaki, R. Miyoshi, T. Ohnuma, W. Sugimoto, Y. Murakami, Chem. Commun. (2001) 341.

[12] Y. Takasu, T. Kawaguchi, W. Sugimoto, Y. Murakami, Electrochim. Acta 48 (2003) 3861.

[13] Y. Takasu, W. Sugimoto, Y. Murakami, Catal. Surveys Asia 7 (2003) 21.

[14] Y. Takasu, H. Itaya, T. Kawaguchi, W. Sugimoto, Y. Murakami, Stud. Surf. Sci. Catal. 145 (2003) 279.

[15] T. Kawaguchi, W. Sugimoto, Y. Murakami, Y. Takasu, Electrochem. Commun., 6 (2004) 480.

[16] H.N. Dinh, X. Ren, F.H. Garzon, P. Zelenay, S. Gottesfeld, J. Electroanal. Chem. 491 (2000) 222.

[17] A.V. Tripkovíc, K.D. Popovíc, B.N. Grgur, B. Blizanac, P.N. Ross, N.M. Markovíc, Electrochim. Acta 47 (2002) 3707.

[18] C. Roth, N. Marty, F. Hahn, J.-M. Léger, C. Lamy, H. Fuess, J. Electrochem. Soc. 149 (2002) E433.

[19] J.O'M. Bockris, H. Wroblowa, J. Electroanal. Chem. 7 (1964) 428.

[20] M. Watanabe, M. Motoo, J. Electroanal. Chem. 60 (1975) 267.

[21] M. Watanabe, S. Motoo, Denki Kagaku (presently Electrochemistry) 41 (1973) 190.

[22] T. Yajima, H. Uchida, M. Watanabe, J. Phys. Chem. B. 108 (2004) 2654.

[23] E. Ticanelli, J.G. Beery, M.T. Paffett, S. Gottesfeld, J. Electroanal. Chem. 258 (1989) 61.

[24] X. Ren, P. Zelenay, S. Thomas, J. Davey, S. Gottesfeld, J. Power Sources 86 (2000) 111.

[25] A.N. Haner, P.N. Ross, U. Bardi, A. Atrei, J. Vac. Sci. Technol. A 10 (1992) 2718.

[26] H.A. Gasteiger, N. Markovíc, P.N. Ross, E.J. Cairns, J. Phys. Chem. 98 (1994) 617.

[27] H.A. Gasteiger, N.M. Markovíc, P.N. Ross, J. Phys. Chem. 99 (1995) 8290.

[28] N.M. Markovíc, H.A. Gasteiger, P.N. Ross, X. Jiang, I. Villegas, M.J. Weaver, Electrochim. Acta 40 (1995) 91.

[29] N.M. Markovíc, A. Widelov, P.N. Ross, O.R. Monteiro, I.G. Brown, Catal. Lett. 43 (1997) 166.

[30] B.N. Grgur, N.M. Markovíc, P.N. Ross, J. Phys. Chem. 102 (1998) 2494.

[31] E. Herrero, K. Franaszczuk, A. Wiekowski, J. Phys. Chem. 98 (1994) 5074.

[32] G. Tremiliosi, H. Kim, W. Chrzanowski, A. Wieckowski, B. Grzybowska, P. Kulesza, J. Electroanal. Chem. 467 (1999) 143.

[33] P. Waszczuk, A. Wieckowski, P. Zelenay, S. Gottesfeld, C. Coutanceau, J.M. Leger, C. Lamy, J. Electroanal. Chem. 511 (2001) 55.

[34] P. Waszczuk, G.-Q. Lu, A. Wieckowski, C. Lu, C. Rise, R.I. Masel, Electrochim. Acta 47 (2002) 3637.

[35] J. Munk, P.A. Christensen, A. Hamnett, E. Skou, J. Electroanal. Chem. 401 (1996) 215.

[36] A. Hamnett, In Interfacial Electrochemistry: Theory, Experiment, and Applications; Wieckowski, A., Ed.; Marcel Dekker: New York, 1999; pp 843-883.

[37] J. C. Davies, B.E.; Hayden, D. Pegg, J. Surf. Sci. 467 (2000) 118.

[38] J.C. Davies, B.E. Hayden, D.J. Pegg, M.E. Rendall, Surf. Sci. 496 (2002) 110.

[39] H.F. Octjen, V.M. Schmidt, U. Stimming, F. Trila, J. Electrochem. Soc. 143

(1996) 3838.

[40] S. Mukerjee, J. McBreen, J. Electrochem. Soc. 146 (1999) 600.

[41] S. Wasmus, A. Kuver, J. Electroanal. Chem. 461 (1999) 14.

[42] H. Wang, C. Wingender, H. Baltruschat, M. Lopez, M.T. Reetz, J. Electroanal. Chem. 509 (2001) 163.

[43] L. Giorgi, A. Pozio, C. Bracchini, R. Giorgi, S. Turtu, J. Appl. Electrochem. 31 (2001) 325.

[44] A.S. Aricò, P.L. Antonucci, E. Modica, V. Baglio, H. Kim, V. Antonucci, Electrochim. Acta 47 (2002) 3723.

[45] S. Swathirajan, Y. Mikhail, J. Electrochem. Soc. 138 (1991) 1321.

[46] M. Watanabe, S. Motoo, J. Electroanal. Chem. 60 (1975) 275.

[47] M. Watanabe, Y.M. Zhu, H. Igarashi, H. Uchida, Electrochemistry 68 (2000) 244.

[48] H. Igarashi, T. Fujino, Y.M. Zhu, H. Uchida, M. Watanabe, Phys. Chem. Chem. Phys. 3 (2001) 306.

[49] T. Iwasita, F.C. Nart, W. Vielstich, Ber. Bunsen-Ges. Phys. Chem. 94 (1990) 1030.

[50] M. Krausa, W. Vielstich, J. Electroanal. Chem. 379 (1994) 307.

[51] W.F. Lin, M.S. Zei, M. Eiswirth, G. Ertl, T. Iwasita, W. Vielstich, J. Phys. Chem. 103 (1999) 6968.

[52] T. Iwasita, Electrochim. Acta 47 (2002) 3663.

[53] P.A. Christensen, A. Hamnett, G.L. Troughton, J. Electroanal. Chem. 362 (1993) 207.

[54] A. Hamnett, Catal. Today 38 (1997) 445.

[55] R. Liu, H. Iddir, Q. Fan, G. Hou, A. Bo, K.L. Ley, E.S.; Smotkin, Y.-E. Sung, H. Kim, S. Thomas, A. Wieckowski, J. Phys. Chem. B 104 (2000) 3518.

[56] P. Waszczuk, G.U. Lu, A. Wieckowski, C. Lu, C. Rice, M.I. Masel, Electrochim. Acta 47 (2002) 36.

[57] C. Lu, C. Rice, M.I. Masel, P.K. Babu, P. Waszczuk, H.S. Kim, E. Oldfield, A. Wieckowski, J. Phys. Chem. B 106 (2002) 9581.

[58] T. Frelink, W. Visscher, J.A.R. van Veen, Electrochim. Acta 39 (1994) 1871.

[59] T. Frelink, W. Visscher, J.A.R. van Veen, Surf. Sci. 335 (1995) 353.

[60] T. Frelink, W. Visscher, J.A.R. van Veen, Langmuir 12 (1996) 3702.

[61] M.M.P. Janssen, J. Moolhuysen, Electrochim. Acta 21 (1976) 869.

[62] H.A. Gasteiger, N. Markovíc, P.N. Ross, E.J. Cairns, J. Phys. Chem. 97 (1993) 12020.

[63] P. Wolohan, P.C.H. Mitchell, D. Thompsett, S.J. Cooper, J. Mol. Catal. A 119 (1997) 223.

[64] F.B. deMongeot, M. Scherer, B. Gleich, E. Kopatzki, R.J. Behm, Surf. Sci. 411 (1998) 249.

[65] S.J. Lee, S. Mukerjee, E.A. Ticianelli, J. McBreen, Electrochim. Acta 44 (1999) 3283.

[66] E. Christofferson, P. Liu, A. Ruban, H.L. Skriver, J.K. Nørskov, J. Catal. 199 (2001) 123.

[67] M. Watanabe, M. Shibata, S. Motoo, J. Electroanal. Chem. 206 (1986) 197.

[68] M. Ciureanu, H. Wang, J. New Mater. Electrochem. Syst. 3 (2000) 107.

[69] J.T. Mueller P.M. Urban, J. Power Sources 75 (1998) 139.

[70] J.T. Müller, P.M. Urban, W.F. Hölderich, J. Power Sources 84 (1999) 157.

[71] R.E. Melnick, G.T.R. Palmore, J. Phys. Chem. 105 (2001) 1012.

[72] J.C. Amphlett, B.A. Peppley, E. Halliop, A. Sadiq, J. Power Sources 96 (2001) 204.

[73] I.-M. Hsing, X. Wang, Y.-J. Leng, J. Electrochem. Soc. 149 (2002) A615.

[74] Y.-C. Liu, X.-P. Qiu, W.-T. Zhu, G.-S. Wu, J. Power Sources 114 (2003) 10.

[75] H. Fukunaga, T. Ishida, N. Teranishi, C. Arai, K. Yamada, Electrochim. Acta 49 (2004) 2123.

[76] T.J. Schmidt, M. Noeske, H.A. Gasteiger, R.J. Behm, P. Britz, H.J. Bönnemann, Electrochem. Soc. 145 (1998) 925.

[77] T.J. Schmidt, H.A. Gasteiger, G.D. Stäb, P.M. Urban, D.M. Kolb, R.J. Behm, J. Electrochem. Soc. 145 (1998) 2354.

[78] C. Lu, R.I. Masel, J. Phys. Chem. B 105 (2001) 9793.

[79] P. Liu, J.K. Nørskov, Fuel Cells 1 (2001) 192.

FIGURE CAPTIONS

Figure 1. Pre-adsorbed CO (CO_{ad}) stripping voltammograms on (a) Pt/C and (b) PtRu/C in 0.5 M H_2SO_4 (60°C).

Figure 2. Complex-plane impedance plots of Pt/C in 1.0 M CH_3OH + 0.5 M H_2SO_4 (60°C) at various electrode potentials. Electrode potentials are shown versus the RHE scale. The solid lines represent the fitted data to the equivalent circuit Fig. 7b.

Figure 3. Complex-plane impedance plots of PtRu/C in 1.0 M CH_3OH + 0.5 M H_2SO_4 (60°C) at various electrode potentials. Electrode potentials are shown versus the RHE scale. The solid lines represent the fitted data to the equivalent circuit Fig. 7b.

Figure 4. Bode plots of Pt/C in 1.0 M CH_3OH + 0.5 M H_2SO_4 (60°C) at various electrode potentials. Electrode potentials are shown versus the RHE scale. The solid lines represent the fitted data to the equivalent circuit Fig. 7b.

Figure 5. Bode plots of PtRu/C in 1.0 M CH_3OH + 0.5 M H_2SO_4 (60°C) at various electrode potentials. Electrode potentials are shown versus the RHE scale. The solid lines represent the fitted data to the equivalent circuit Fig. 7b.

Figure 6. The characteristic frequency where the phase angle deviates from ~90° in the Bode plots F_1 as a function of the applied electrode potential for Pt/C (open circles) and PtRu/C (open squares) and the frequency where the phase angle nears zero in the Bode plots F_2 as a function of the applied electrode potential for Pt/C (solid circles) and PtRu/C (solid squares).

Figure 7. (a) Equivalent circuit for modeling the Faradaic impedance on DMFC anodes. (b) Equivalent circuit for modeling the Faradaic impedance on DMFC anodes considering the high frequency impedance data.

Figure 8. The (a) reaction resistance of CH_3OH oxidation to CO_{ad} (R_∞) and (b) the reaction resistance (R_0) and (c) inductance of CO_{ad} oxidation (L) as a function of the

electrode potential on Pt/C (circles) and PtRu/C (squares) in 1.0 M CH_3OH + 0.5 M H_2SO_4 obtained by fitting the impedance data using the equivalent circuit in Fig. 7b.

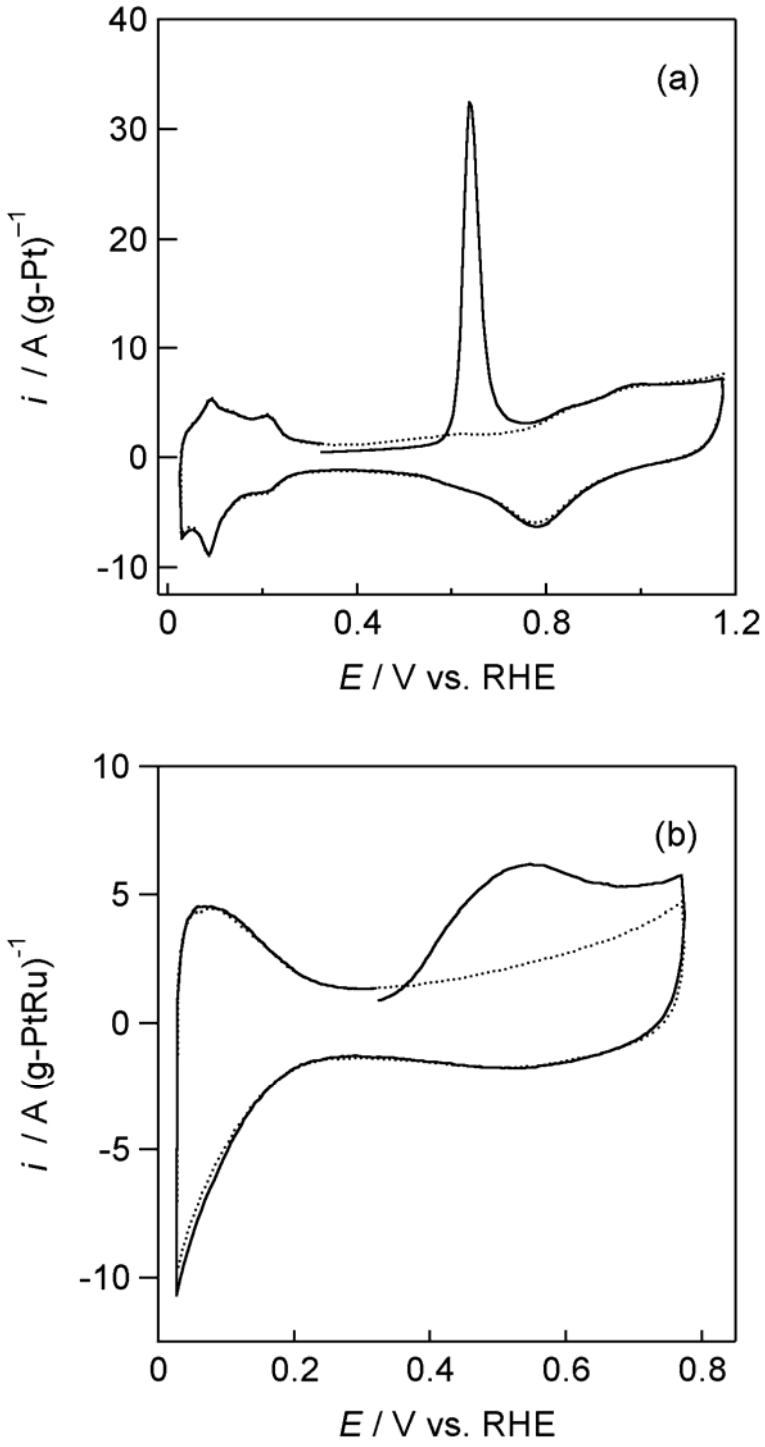

Figure 1. Pre-adsorbed CO (CO_{ad}) stripping voltammograms on (a) Pt/C and (b) PtRu/C in 0.5 M H_2SO_4 (60°C).

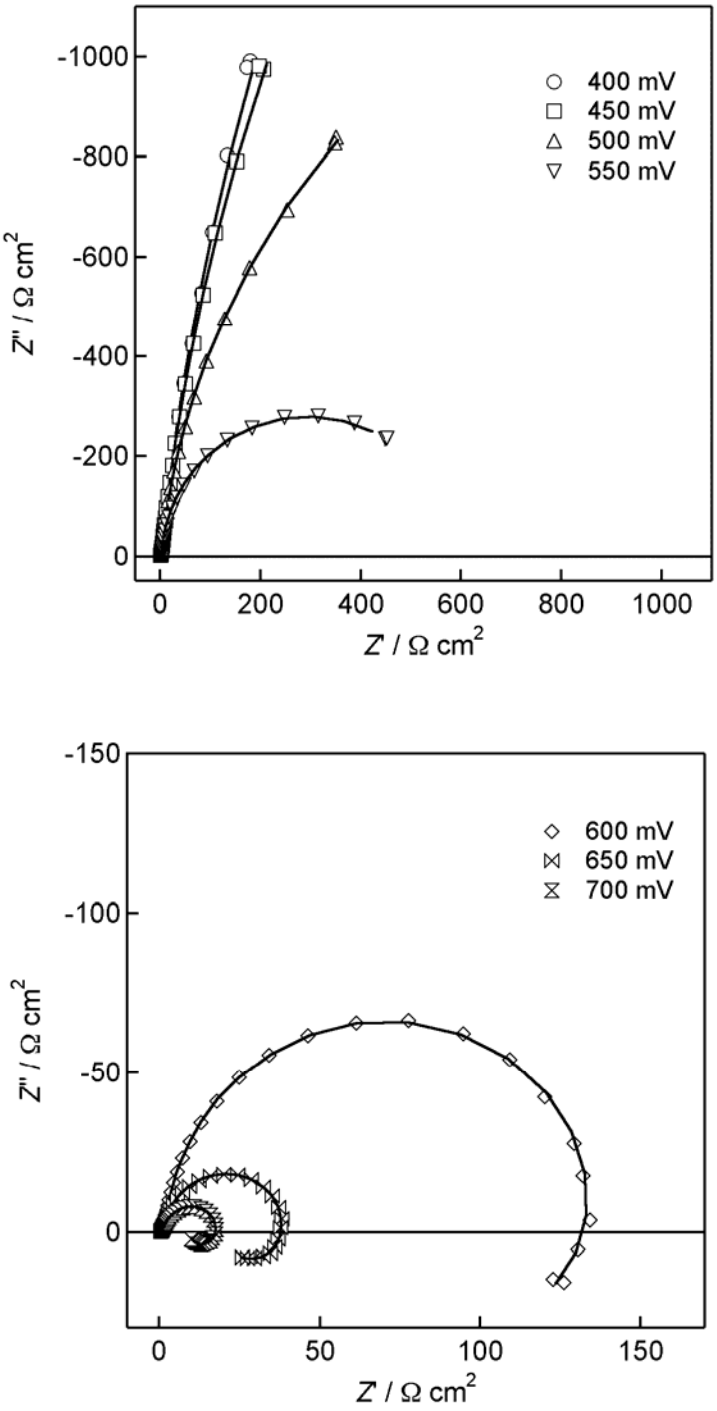

Figure 2. Complex-plane impedance plots of Pt/C in 1.0 M CH_3OH + 0.5 M H_2SO_4 (60°C) at various electrode potentials. Electrode potentials are shown versus the RHE scale. The solid lines represent the fitted data to the equivalent circuit Fig. 7b.

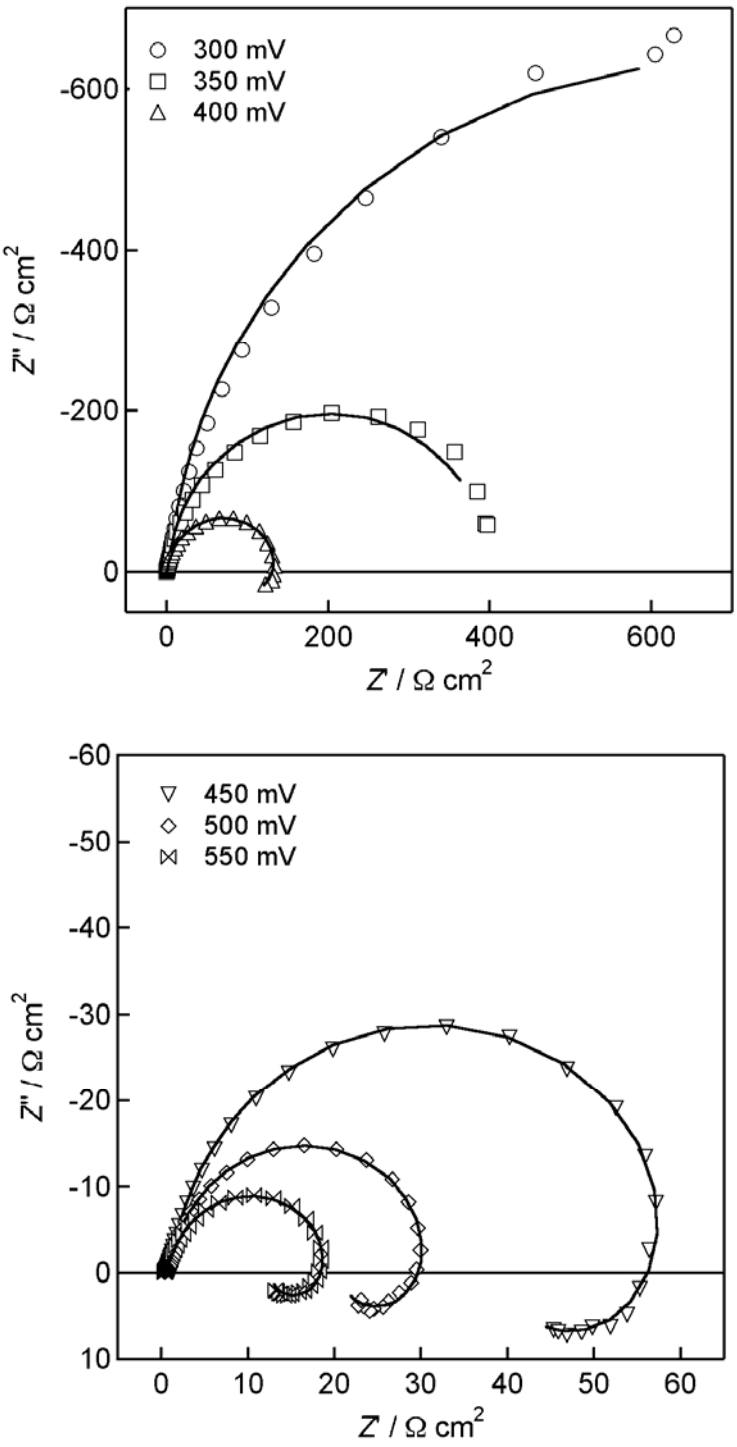

Figure 3. Complex-plane impedance plots of PtRu/C in 1.0 M CH_3OH + 0.5 M H_2SO_4 (60°C) at various electrode potentials. Electrode potentials are shown versus the RHE scale. The solid lines represent the fitted data to the equivalent circuit Fig. 7b.

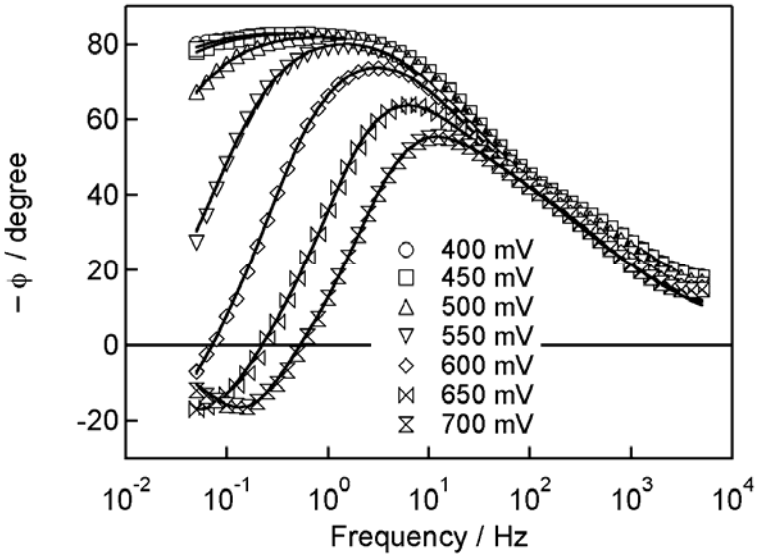

Figure 4. Bode plots of Pt/C in 1.0 M CH_3OH + 0.5 M H_2SO_4 (60°C) at various electrode potentials. Electrode potentials are shown versus the RHE scale. The solid lines represent the fitted data to the equivalent circuit Fig. 7b.

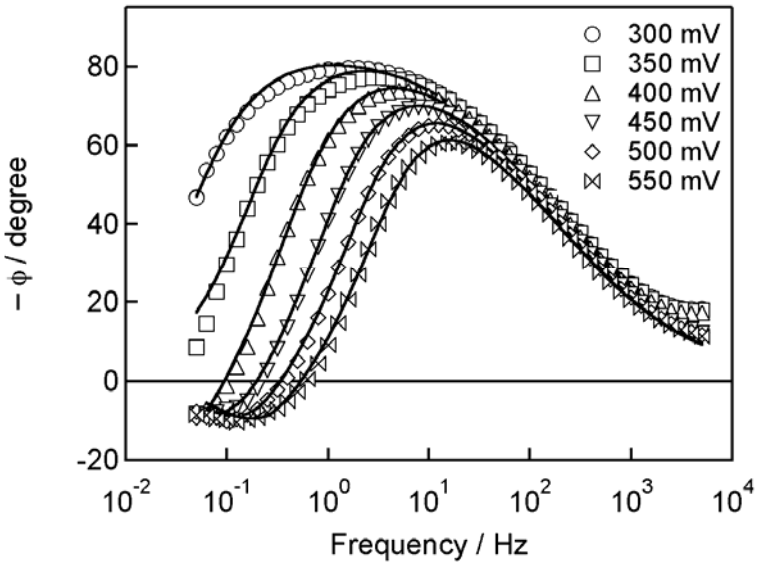

Figure 5. Bode plots of PtRu/C in 1.0 M CH_3OH + 0.5 M H_2SO_4 (60°C) at various electrode potentials. Electrode potentials are shown versus the RHE scale. The solid lines represent the fitted data to the equivalent circuit Fig. 7b.

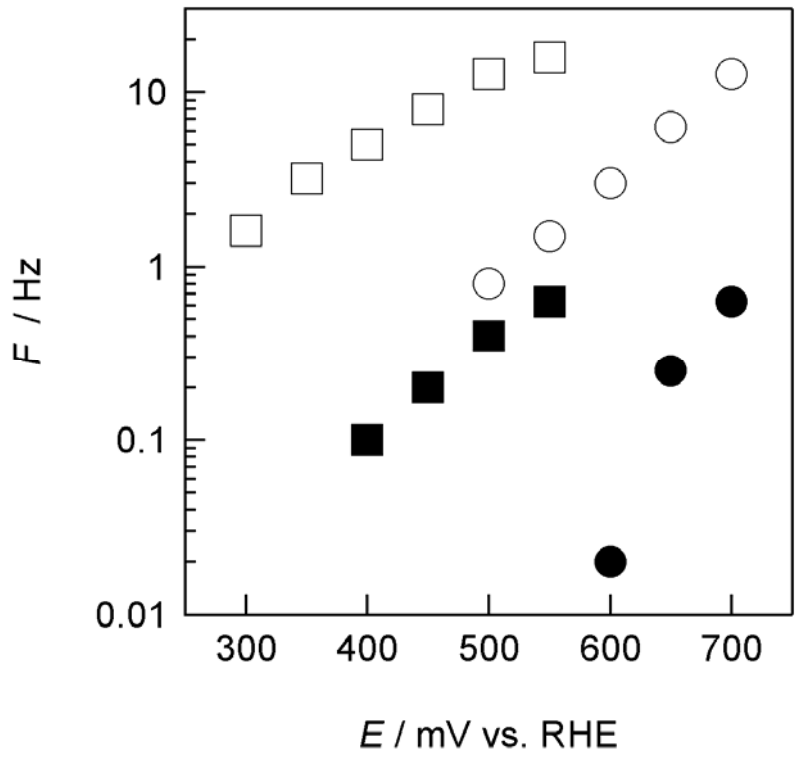

Figure 6. The characteristic frequency where the phase angle deviates from ~90° in the Bode plots F_1 as a function of the applied electrode potential for Pt/C (open circles) and PtRu/C (open squares) and the frequency where the phase angle nears zero in the Bode plots F_2 as a function of the applied electrode potential for Pt/C (solid circles) and PtRu/C (solid squares).

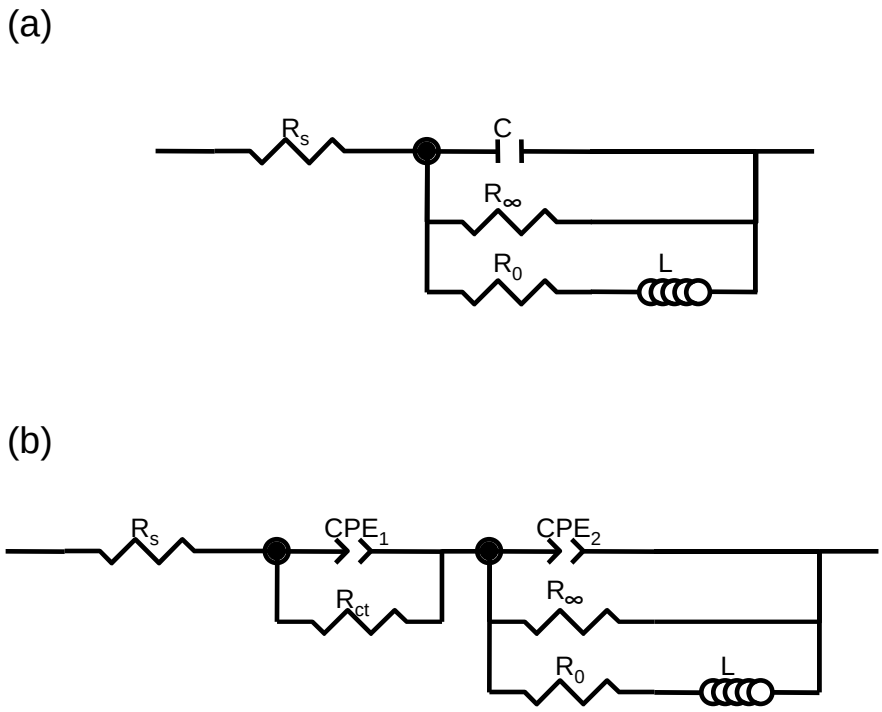

Figure 7. (a) Equivalent circuit for modeling the Faradaic impedance on DMFC anodes. (b) Equivalent circuit for modeling the Faradaic impedance on DMFC anodes considering the high frequency impedance data.

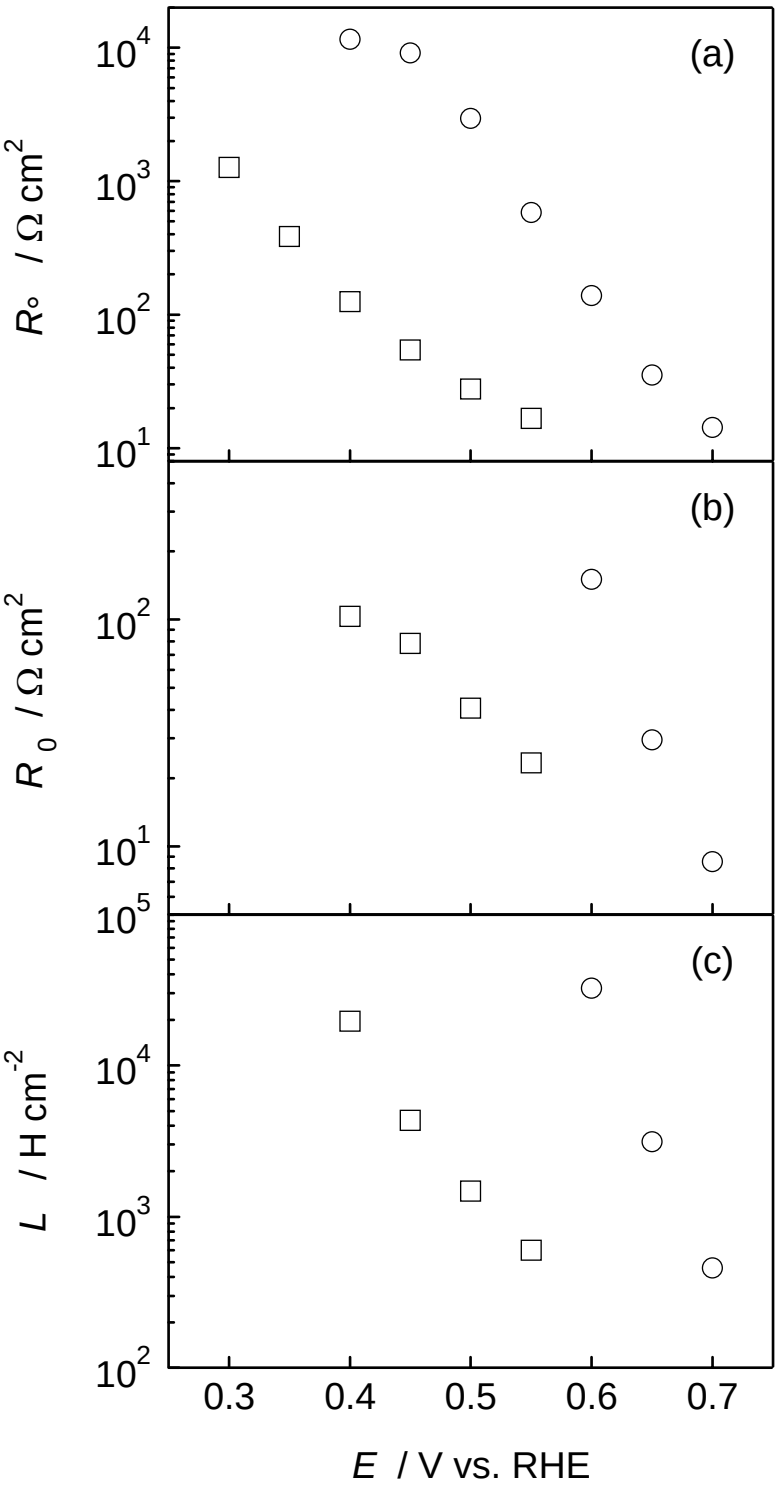

Figure 8. The (a) reaction resistance of CH_3OH oxidation to CO_{ad} (R_∞) and (b) the reaction resistance (R_0) and (c) inductance of CO_{ad} oxidation (L) as a function of the electrode potential on Pt/C (circles) and PtRu/C (squares) in 1.0 M CH_3OH + 0.5 M H_2SO_4 obtained by fitting the impedance data using the equivalent circuit in Fig. 7b.